Observation of Standing Waves of Electron-Hole Sound in a Photoexcited Semiconductor

P. Padmanabhan,[1,2] S. M. Young,[1,2] M. Henstridge,[1,2] S. Bhowmick,[1,3] P. K. Bhattacharya,[1,3] and R. Merlin[1,2]

[1]*Center for Photonics and Multiscale Nanomaterials, University of Michigan, Ann Arbor, Michigan 48109, USA*

[2]*Department of Physics, University of Michigan, Ann Arbor, Michigan 48109-1040, USA*

[3]*Department of Electrical Engineering and Computer Science, University of Michigan, Ann Arbor, Michigan 48109-2122, USA*

(Received 22 April 2014; published 8 July 2014)

Three-dimensional multicomponent plasmas composed of species with very different masses support a new branch of charge-density fluctuations known as acoustic plasmons. Here, we report on an ultrafast optical method to generate and probe coherent states of acoustic plasmons in a slab of GaAs, which relies on strong photoexcitation to create a large population of light electrons and heavy holes. Consistent with the random-phase-approximation theory, the data reveal standing plasma waves confined to these slabs, similar to those of conventional sound but with associated velocities that are significantly larger.

DOI: 10.1103/PhysRevLett.113.027402 PACS numbers: 78.66.-w, 71.45.Gm, 72.10.Di, 78.47.jh

The collective behavior of a system of charged particles leads to the emergence of new longitudinal excitations known as plasmons. Because the plasma particles interact through long-range Coulomb forces, in the three-dimensional case, the frequency of such excitations, known as optical plasmons, does not vanish in the long-wavelength limit [1]. Unlike single-component plasmas, such as that of electrons in a metal, multicomponent plasmas can sustain acoustic modes in addition to optical plasmons [2,3]. For two-component systems, a large difference in mass between the carriers is thought to be a sufficient condition for the existence of these soundlike modes [2,3,4], which can be envisioned as a collective oscillation where the light particles provide a restoring force proportional to the square of the wave vector by adiabatically screening the heavy particles. Not to be confused with similarly named modes of metallic surfaces [5,6] or two-dimensional systems [7,8], acoustic plasmons (APs) have long attracted considerable attention as a possible source of high-temperature superconductivity [3,9] because the corresponding velocity should be much larger than that of conventional sound.

Owing to the narrow parameter span in which long-lived APs are expected to occur [3], they have only been identified in a handful of systems including gas plasmas [10] and, notably, in GaAs using spontaneous Raman scattering [11]. Here, we report on the observation of APs in photoexcited GaAs using coherent optical methods and femtosecond laser sources. The large peak powers delivered by such sources and their coherence allow, respectively, the exploration of a range of densities that is significantly larger than in previous investigations [11] and the generation of AP coherent states through stimulated emission. The results show that AP waves generated in a thin slab of GaAs behave like those of classical sound or light resonators in that they are standing waves confined to the slab. The data also reveal evidence that the primary driver for the coherent generation of AP waves is their coupling to phonon coherent states.

Photoexcited GaAs is an ideal choice in a search for APs due to the large mismatch between the heavy-hole and electron effective masses ($m_{hh}/m_{lh} = 6.7$) [12]. Ultrafast optical experiments were performed on layered structures, grown by molecular beam epitaxy, in which the key constituents were GaAs slabs of thicknesses d ranging from 1150–6000 Å (see the inset of Fig. 1). Two thin AlAs claddings prevented photoexcited carriers from leaving the active GaAs layer. Pump-probe differential reflectivity experiments were performed at ~10 K using a two-pump sequence consisting of a ~75 fs infrared (IR) pulse (1.55 eV) followed by a ~300 fs visible pulse (1.92 eV). A single probe, with characteristics identical to the IR pump, was scanned across a range of time delays relative to the IR pump using a mechanical delay line. The two pumps served both to photoexcite the sample and to generate coherent charge-density fluctuations. These fluctuations cause oscillatory changes in the optical constants that were measured by monitoring accompanying changes in the reflectivity of the probe pulse using electro-optic sampling. At comparable fluences, the coherent oscillations associated with phonons were generated primarily by the IR pulses, as the phonon period was longer than the IR pulse width but shorter than that of the visible pulse. In contrast, the photoexcited (electron or total hole) carrier density N was significantly greater for excitation with the visible pulses since their photon energy was well above the fundamental gap

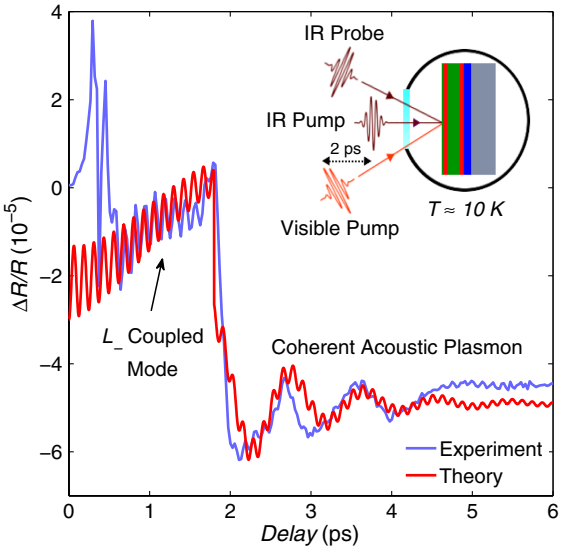

FIG. 1 (color online). Time-domain differential-reflectivity trace (blue curve) recorded at average laser powers of 15 (IR pump), 12 (visible pump), and 5 mW (IR probe). The oscillations at ~8 THz are due to the L_- mode. The AP states manifest themselves as the much slower oscillations triggered by the arrival of the visible pulses, ~1.8 ps after the initial IR pump excitation. The red curve represents the solution to the coupled-oscillator model described in the text at $N = 3.4 \times 10^{19}$ cm^{-3} for $F_0 = 0.22 \times 10^{23}$. $\beta = 7.5 \times 10^{11}$ rad/s, $\omega_{L_-} = 8.096$ THz, $\gamma_{L_-} = 1.0 \times 10^{12}$ rad/s, and $\gamma_{AP} = 2.0 \times 10^{12}$ rad/s (a constant term equal to -0.30×10^{-4} was added after a delay of 1.8 ps). The inset shows the experimental geometry, temporal sequence of pulses, and a sketch of the samples. Each of the sample structures are comprised of a n^+ (001) GaAs substrate (gray), 200-nm-thick $Al_{0.8}Ga_{0.2}As$ buffer layer (blue), followed by an active GaAs layer (green) of thickness d sandwiched between AlAs layers of thicknesses 50 and 10 nm (red), and a 8-nm-thick GaAs top cap layer (green).

(~1.52 eV) and resonant with the $E_0 + \Delta_0$ gap of GaAs. From the experimental pump fluences, frequencies, skin depth, and reflectivity obtained from the optical constants of GaAs, N was calculated [13] to be in the range $3.7 \times 10^{18} - 3.6 \times 10^{19}$ cm^{-3}, nearly 2 orders of magnitude larger than what can be achieved with continuous-wave laser sources [11].

Typical time-domain data are shown in Fig. 1. Zero time delay is defined by the moment at which the IR pump and probe pulses simultaneously arrive at the sample. At delays < 1.8 ps (before the arrival of the visible pump), pronounced IR-pump-induced ~8 THz oscillations in the reflectivity were observed. These are due to the formation of coherent states associated with the lower, L_- branch of the coupled modes resulting from the interaction between optical plasmons and longitudinal-optical phonons [14], as also seen in n^+-GaAs [15]. Similar oscillations were observed in all the structures. Coincident with the arrival of the visible pump at ~1.8 ps, the differential reflectivity trace in Fig. 1 exhibits a steplike shift, due to the sudden increase in the density of photoexcited carriers, followed by a large-amplitude, rapidly decaying oscillation with frequency ~1.15 THz. This oscillation frequency is far below those of the optical phonons, and 50–100 times higher than that of acoustic phonons at the probed wave vector. We ascribe such oscillations to coherent density fluctuations associated with confined APs, which decay rapidly through Landau damping due to their coupling to the continuum of single-particle excitations [14]. As shown in Fig. 2, differential reflectivity traces for a variety of carrier densities reveal that the oscillation frequency ω has an N^η dependence, with $\eta = 0.5 \pm 0.2$. As shown later, this dependence is consistent with theoretical predictions based on the random-phase approximation (RPA).

The geometry of our experiments probed only charge-density fluctuations [16], the spectrum of which is defined by the zeroes of the longitudinal dielectric function of the photoexcited plasma, ε_L. Within the RPA [14],

$$\varepsilon_L(\mathbf{q},\omega) = \varepsilon_\infty + 4\pi[\chi_e(\mathbf{q},\omega) + \chi_{hh}(\mathbf{q},\omega) + \chi_{lh}(\mathbf{q},\omega) + \chi_{hh,lh}(\mathbf{q},\omega) + \chi_L(\mathbf{q},\omega)]. \quad (1)$$

Here, ω and $\mathbf{q}$ are the frequency and the wave vector of the perturbation to which the plasma responds and ε_∞ is a constant that accounts for higher-frequency transitions. χ_L is the lattice susceptibility given by [17]

$$\chi_L = \frac{\varepsilon_\infty}{4\pi} \frac{\omega_{LO}^2 - \omega_{TO}^2}{\omega_{TO}^2 - \omega^2 - i\gamma\omega}, \quad (2)$$

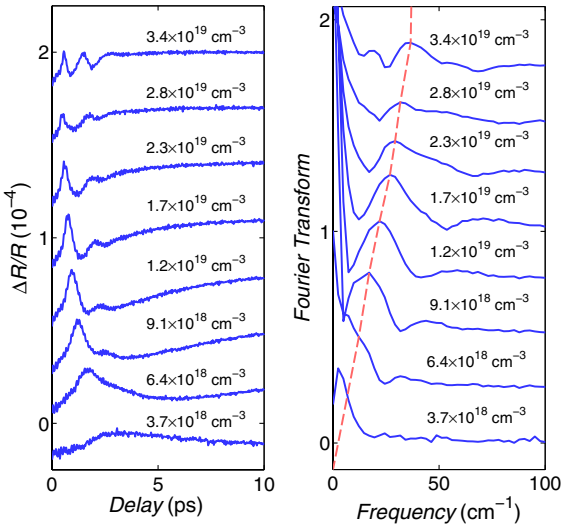

FIG. 2 (color online). Time-domain results for the 1500-Å-thick GaAs sample showing AP oscillations at various N (left panel) and corresponding Fourier transforms (right panel). The origin of time delays coincides with the arrival of the visible pump pulses. The dashed red curve is a visual guide that indicates the AP feature. Curves have been shifted vertically for clarity purposes.

where $\gamma = 5\ \mathrm{cm}^{-1}$ is the phonon damping constant, $\omega_{\mathrm{LO}} = 295\ \mathrm{cm}^{-1}$ is the LO phonon frequency and $\omega_{\mathrm{TO}} = 272\ \mathrm{cm}^{-1}$ is the transverse-optical (TO) phonon frequency at low temperatures. χ_e, χ_{hh}, and χ_{lh} are the intraband susceptibilities of electrons, heavy, and light holes, respectively, and $\chi_{hh,lh}$ is the interband contribution associated with transitions between the two hole bands. The carrier susceptibilities depend on the distribution of photoexcited electrons and holes among all conduction- and valence-band states throughout the Brillouin zone. It is assumed that, following a rapid transition into quasi-equilibrium states, the carriers populate the bands according to Fermi-Dirac distributions with the same effective temperature for electrons and holes, and the same chemical potential for the two hole species. Thus, the intraband susceptibilities can be calculated using the Lindhard-Mermin model [14,18] with the result

$$\chi_j(\mathbf{q},\omega) = \frac{(1+i\Gamma/\omega)\chi_j^0(\mathbf{q},\Omega)}{1+(i\Gamma/\omega)\chi_j^0(\mathbf{q},\Omega)/\chi_j^0(\mathbf{q},0)}, \tag{3}$$

where Γ is the collisional damping rate of the plasma, $\Omega = \omega + i\Gamma$, and

$$\chi_j^0(\mathbf{q},\Omega) = \frac{e^2}{4\pi^3 q^2}\int C_j\left[\frac{f_j(\mathbf{k},T)-f_j(\mathbf{k}+\mathbf{q},T)}{E_j(\mathbf{k}+\mathbf{q})-E_j(\mathbf{k})-\hbar\Omega}\right]d\mathbf{k} \tag{4}$$

is the RPA intraband susceptibility [19,20]. Here, $f_j(\mathbf{k},T)$ is the Fermi-Dirac distribution function and C_j is the square of the intraband transition matrix element of the jth species with $C_e = 1$ and [19,20,21]

$$C_{hh} = C_{lh} = \frac{1}{4} + \frac{3(k^2+\mathbf{q}\cdot\mathbf{k})^2}{4k^2(q^2+k^2+2\mathbf{q}\cdot\mathbf{k})} \tag{5}$$

The interband susceptibility associated with $hh-lh$ transitions can also be written using Eq. (3), provided χ_j^0 is replaced by the RPA interband susceptibility [19,20]

$$\chi_{hh,lh}^0(\mathbf{q},\Omega) = \frac{e^2}{4\pi^3 q^2}\int d\mathbf{k} C_{hh,lh} \times \sum_{j=1}^{2}\frac{f_{lh}(\mathbf{k},T)-f_{hh}(\mathbf{k}+\mathbf{q},T)}{E_{hh}(\mathbf{k}+\mathbf{q})-E_{lh}(\mathbf{k})+(-1)^j\hbar\Omega}, \tag{6}$$

where $C_{hh,lh} = 1 - C_{hh} = 1 - C_{lh}$ [19,20,21]. In the sum, $j = 1$ ($j = 2$) corresponds to light-to-heavy (heavy-to-light) hole transitions. In all the calculations, the carrier energies appearing in Eqs. (4) and (6) were computed using a 30-band $\mathbf{k}\cdot\mathbf{p}$ model [22].

Since the changes in the probe reflectivity are determined by the spontaneous Raman tensor [23], the experimental results are compared with the electron dynamic structure factor

$$S_e(\omega,\mathbf{q}) = q^2\mathrm{Im}\left[\chi_e(\omega,\mathbf{q}) - \frac{4\pi\chi_e^2(\omega,\mathbf{q})}{\varepsilon_L(\omega,\mathbf{q})}\right], \tag{7}$$

which is proportional to the Raman cross section when the electron mass is much smaller than those of the holes [14]. As such, S_e gives not only the frequency and lifetime of the plasma quasiparticles (as $1/\varepsilon_L$ does), but also a good estimate of the relative oscillation amplitudes of the various modes. Figure 3 shows an example of the calculated S_e for $N = 2.2\times10^{19}\ \mathrm{cm}^{-3}$. The AP is associated with the relatively broad band peaked at a frequency that depends linearly with q. This corresponds to an acoustic mode with a velocity of ~300 km/s, which is 50–100 times larger than that of conventional sound in GaAs. The narrower peak at ~270 cm^{-1} is due to the L_- mode.

Similar to the acoustic and electromagnetic counterpart problems, a slab is expected to support a discrete array of AP modes defined by the set of wave vectors for which the corresponding waves match specific boundary conditions. Classically, the plasma can be treated as a fluid [24], allowing boundary conditions to be derived from the requirement that the normal component of the fluid velocity vanish at the slab edges. This condition may be combined with the linearized form of the one-dimensional continuity equation relevant to the slab geometry, given by

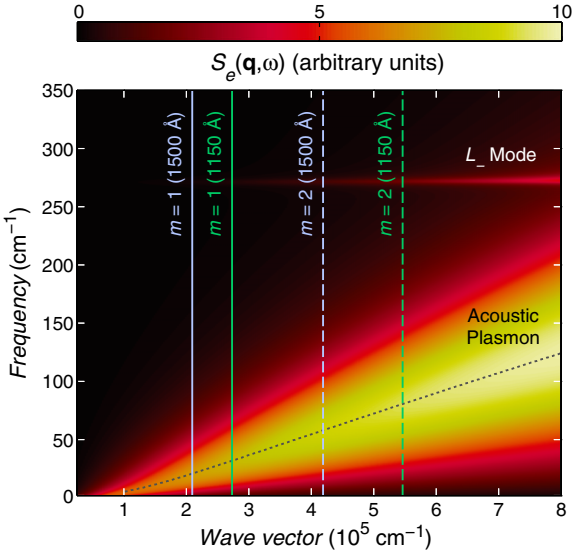

FIG. 3 (color online). Contour plot of S_e vs (ω, q) for an electron-hole plasma of density $N = 2.2\times10^{19}\ \mathrm{cm}^{-3}$. The effective carrier temperature is $T = 400$ K and $\Gamma = 5.9$ meV. The dominant source of scattering is the acoustic plasmon; the dotted line denotes the position of the maximum of the corresponding band. Also shown is the band corresponding to the L_- mode. Vertical lines indicate the wave vectors associated with the $m = 1$ (solid) and $m = 2$ (dashed) modes of the standing AP waves for samples with active regions of thicknesses 1500 (white) and 1150 Å (green).

$$\frac{\partial \delta N}{\partial t} + N_0 \frac{\partial v_z}{\partial z} = 0, \tag{8}$$

where z is the direction normal to the slab, t is the time, $v_z(z,t)$ is the z component of the fluid velocity, and $N(z,t) = N_0 + \delta N$ is the carrier density with $\delta N \ll N_0$. For a slab defined by $0 < z < d$, the density fluctuation takes the form of standing waves

$$\delta N \propto \cos(q_m z)\sin(\omega t + \phi) \tag{9}$$

with allowed wave vectors $q_m = m\pi/d$, where m is a positive integer.

The vertical lines in Fig. 3 represent the allowed wave vectors of the two lowest confined AP modes for the slabs with $d = 1150$ and 1500 Å, at a fixed density. Comparison between the theoretical and experimental N dependence of the two lowest-order standing modes for these samples is shown in Fig. 4. The values of N, carrier temperature ($T = 400$ K), and damping ($\Gamma = 5.9$ meV) used in the calculations were inferred from experimental and theoretical parameters [25,26]. As shown in Fig. 4(a) for $d = 1500$ Å, the measured N dependence of the oscillation frequency is in good agreement with that of the $m = 1$ confined mode ($q = 2.1 \times 10^5$ cm^{-1}). This also applies to the $d = 1150$ Å sample [Fig. 4(b)], which exhibits two separate oscillations at frequencies close to those of the $m=1$ ($q_1 = 2.7\times 10^5$ cm^{-1}) and $m=2$ ($q_2 = 5.4 \times 10^5$ cm^{-1}) standing waves. The calculated N dependence of the AP frequency is approximately of the form N^η with $\eta = 0.3$–0.4, depending on the wave vector. These RPA values are consistent with the experimental data ($\eta = 0.5 \pm 0.2$), as well as the $\eta = 1/3$ behavior expected for plasmas with two carriers of very different masses [2,3]. As seen in the insets of Fig. 4, the width and oscillator strength of the experimental peaks are also in good agreement with the theoretical structure factor. These considerations support our contention that the oscillations that follow the arrival of the visible pump are due to APs.

The substantial decrease in the L_- amplitude that accompanies the onset of the low-frequency oscillations, together with the fact that the AP is only observed when the L_- mode is present, suggests that the AP draws its coherence from the L_- state. This generation process can be modeled by classical equations describing coupled oscillators [27]:

$$\ddot{Q} + \gamma_{L_-}\dot{Q} + \omega_{L_-}^2 Q = F_Q(t) + \beta\sqrt{\omega_{L_-}\omega_{\mathrm{AP}}(t)}\,A, \tag{10a}$$

$$\ddot{A} + \gamma_{\mathrm{AP}}\dot{A} + \omega_{\mathrm{AP}}^2(t)A = F_A(t) + \beta\sqrt{\omega_{L_-}\omega_{\mathrm{AP}}(t)}\,Q. \tag{10b}$$

A (Q) is the amplitude associated with the acoustic plasmon (L_-) mode, F_A (F_Q) is the laser-induced force that drives the acoustic plasmon (L_-) oscillations, and β is a phenomenological coupling constant.

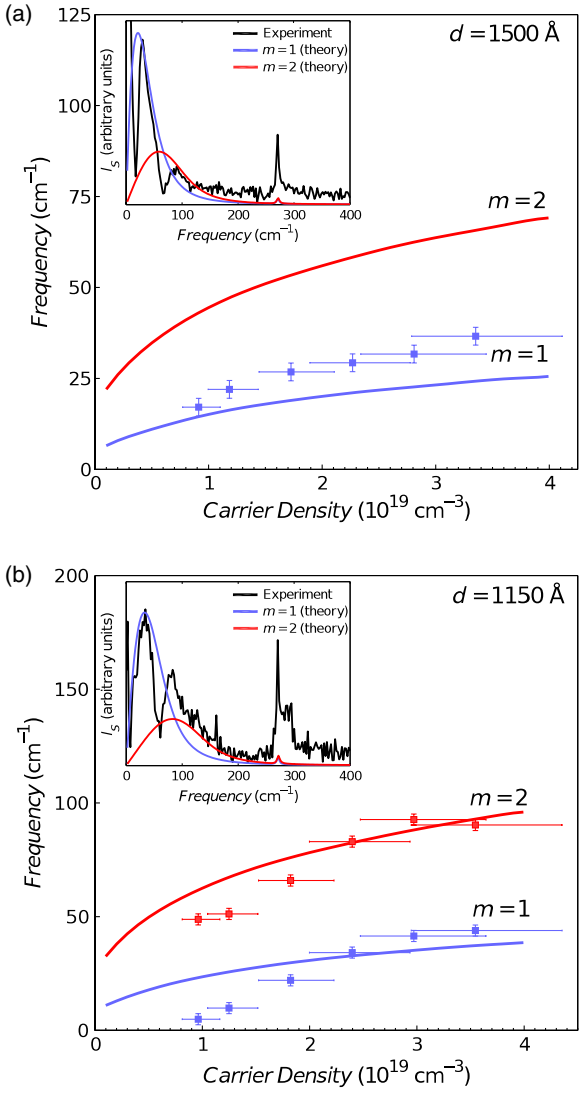

FIG. 4 (color online). Comparison between the measured (dots) and calculated (curves) frequencies of the $m = 1$ (blue) and $m = 2$ (red) confined AP modes as a function of the carrier density. The insets show the theoretical dynamical structure factor for each mode and the Fourier transforms of the measured differential-reflectivity spectra for GaAs slabs of thicknesses (a) $d = 1500$ Å at $N = 2.3 \times 10^{19}$ cm^{-3} (experiments show only the first standing mode) and (b) $d = 1150$ Å at $N = 2.4 \times 10^{19}$ cm^{-3}.

A representative solution of these equations is shown as the red trace in Fig. 1. The good agreement between theory and experiments validates the model. In the calculations, the driving term associated with the IR pump was neglected since the AP oscillations were not observed in the absence of the visible pump and, moreover, because its effect was significantly reduced by using a phase-sensitive detection method where the visible pump was not chopped. The primary role of the visible pump was to increase the AP frequency by dramatically increasing N. Carrier injection

was assumed to follow a simple rate law with the normalized IR and visible pump intensities, thereby imparting a time dependence on ω_{AP} [28]. β and $F_Q(t)$ were treated, respectively, as a free parameter and a steplike function, consistent with the established generation mechanism of coherent phonons in opaque materials [29]. Finally, the signal measured at the detector is the sum of the A and Q contributions, such that $\Delta R/R = r_Q Q + r_A A$. Since r_Q and r_A are not independently known, the effects due to the coupling β and to the difference in scattering efficiency are indistinguishable. Accordingly, r_Q/r_A was set to unity, thereby reducing the parameter space for the model to the determination of β.

In summary, we have generated standing AP waves and probed their behavior using ultrafast optical techniques that extend considerably the range of parameters explored in previous studies. The coherent AP states exhibit a carrier-density and slab-thickness dependence that validates RPA predictions for multicomponent plasmas, and their generation mechanism reveals how they couple to other longitudinal excitations.

Work supported by the MRSEC Program of the National Science Foundation under Grant No. DMR-1120923. R. M. acknowledges support of the Simons Foundation.

[1] P. W. Anderson, *Basic Notions of Condensed Matter Physics* (Addison-Wesley, Reading, MA, 1997), p. 43.
[2] P. Nozières and D. Pines, Phys. Rev. **109**, 1062 (1958).
[3] J. Ruvalds, Adv. Phys. **30**, 677 (1981).
[4] B. Bennacer and A. A. Cottey, J. Phys.: Condens. Matter **1**, 1809 (1989).
[5] B. Diaconescu *et al.*, Nature (London) **448**, 57, (2007).
[6] S. J. Park and A. E. Palmer, Phys. Rev. Lett. **105**, 016801 (2010).
[7] S. J. Allen, D. C. Tsui, and R. A. Logan, Phys. Rev. Lett. **38**, 980 (1977).
[8] F. Stern, Phys. Rev. Lett. **18**, 546 (1967).
[9] H. Fröhlich, J. Phys. C **1**, 544 (1968).
[10] A. Y. Wong, R. W. Motley, and N. D'Angelo, Phys. Rev. **133**, A436 (1964).
[11] A. Pinczuk, J. Shah, and P. Wolff, Phys. Rev. Lett. **47**, 1487 (1981).
[12] U. Rössler, Solid State Commun. **65**, 1279 (1988).
[13] A. Sabbah and D. Riffe, Phys. Rev. B **66**, 165217 (2002).
[14] G. Abstreiter, M. Cardona, and A. Pinczuk, in *Light Scattering in Solids IV*, edited by M. Cardona and G. Guntherodt (Springer, New York, 1984), Chap. 2, p. 5.
[15] K. Ishioka, A. K. Basak, and H. Petek, Phys. Rev. B **84**, 235202 (2011).
[16] J. M. Bao, L. N. Pfeiffer, K. W. West, and R. Merlin, Phys. Rev. Lett. **92**, 236601 (2004).
[17] P. Yu and M. Cardona, *Fundamentals of Semiconductors* (Springer, New York, 2010), 4th ed., Chap. 6, p. 295.
[18] N. D. Mermin, Phys. Rev. B **1**, 2362 (1970).
[19] J. Young and P. Kelly, Phys. Rev. B **47**, 6316 (1993).
[20] W. Bardyszewski, Solid State Commun. **57**, 873 (1986).
[21] M. Combescot and P. Nozières, Solid State Commun. **10**, 301 (1972).
[22] S. Richard, F. Aniel, and G. Fishman, Phys. Rev. B **70**, 235204 (2004).
[23] T. E. Stevens, J. Kuhl, and R. Merlin, Phys. Rev. B **65**, 144304 (2002).
[24] R. J. Goldston and P. H. Rutherford, *Introduction to Plasma Physics* (Taylor & Francis, New York, 1995), Vol. 1.
[25] D. S. Kim and P. Y. Yu, Phys. Rev. B **43**, 4158 (1991).
[26] A. Pinczuk, G. Abstreiter, R. Trommer, and M. Cardona, Solid State Commun. **30**, 429 (1979).
[27] K. Singwi and M. Tosi, Phys. Rev. **147**, 658 (1966).
[28] A. Kuznetsov and C. Stanton, Phys. Rev. B **51**, 7555 (1995).
[29] R. Merlin, Solid State Commun. **102**, 207 (1997).